Journal of Manufacturing Processes 79 (2022) 626–638

Contents lists available at ScienceDirect

Journal of Manufacturing Processes

journal homepage: www.elsevier.com/locate/manpro

Electrical and thermal stability of Al-Cu welds: Performance benchmarking of the hybrid metal extrusion and bonding process☆

Aksel Elkjaer [a,*], Jørgen A. Sørhaug [b], Geir Ringen [a], Ruben Bjørge [c], Øystein Grong [d]

[a] Department of Mechanical and Industrial Engineering, Norwegian University of Science and Technology, Richard Birkelands Vei 2b, 7491 Trondheim, Norway
[b] Department of Physics, Norwegian University of Science and Technology, Trondheim, Norway
[c] Department of Materials and Nanotechnology, SINTEF Industry, Trondheim, Norway
[d] HyBond AS, Trondheim, Norway

ARTICLE INFO

Keywords:
Aluminum
Copper
Intermetallic growth rate
Electrical resistance
Hybrid metal extrusion and bonding

ABSTRACT

Advances in joining processes for aluminum and copper are sought after to facilitate the greater adoption of aluminum in electrical applications. Aluminum's chemical affinity to copper causes the joining and lifetime of Al-Cu welds to be vulnerable to the formation of various intermetallic compounds. Intermetallic compounds and the resulting weld structure are known to reduce the structural integrity and increase the electrical resistance of Al-Cu welds. In this study we evaluate the novel joining process, Hybrid Metal Extrusion and Bonding, for butt welding aluminum and copper. The weld structure was examined using scanning and transmission electron microscopy, and the weld resistance was measured using four-point measurements forecast to the weld interface. Energy dispersive spectroscopy and electron diffraction zone axis patterns were analysed to identify intermetallic compounds. Weld samples were examined pre and post heat treatment at 200 °C, 250 °C and 350 °C for total durations of over 1000 h. The results are compared to existing Al-Cu joining processes, and a new metric, weld interface resistivity, is proposed to compare the electrical properties of bimetallic welds. The Hybrid Metal Extrusion and Bonding process was found to form a thin, consistent and straight intermetallic layer with negligible impact on electrical resistance in the as-welded condition. Artificial ageing of samples by heat treatment established the overall growth rate of intermetallic compounds. The growth rate was used to evaluate the weld's operational lifetime versus temperature. The intermetallic growth rate of Hybrid Metal Extrusion and Bonding was quantified at 200 °C and compared to alternative processes. The Hybrid Metal Extrusion and Bonding process showed a significant performance advantage requiring the longest time to reach 2 μm thickness. Furthermore, the growth of intermetallic compounds did not increase the electrical resistance of the weld interface. The negligible impact on electrical resistance and slow intermetallic growth are promising results of the potential functional performance. This study is the first characterisation of the Hybrid Metal Extrusion and Bonding process for electrical applications showcasing its exciting potential for the joining of aluminum and copper.

1. Introduction

The world's energy diet is changing with increasing consumption of electricity. “Electrification of end uses” is explicit policy for reducing greenhouse gases across the globe [1], and an increasing dependency on electricity is fostering interest in joining two of the best electrical conductors, namely copper and aluminum [2,3]. Copper is ubiquitous in electrical applications due to its good conductance and ease in forming reliable connections. Aluminum, on the other hand, has less favourable connection properties, but offers greater conductivity per unit mass than copper. Hence, aluminum conductors are preferable for lightweight applications in which mass savings compensate for more complex connection methods.

Historically, such lightweight applications using aluminum have been predominantly limited to high voltage power transmission [4,5]. Recently, aluminum conductors have become more desirable with the

☆ This work was supported by the Research Council of Norway's “Aluminium bus bars for marine battery systems” (ES635028), “Value” (267768), the “In-SANE” (301176), NorFab (295864) and the NORTEM (197405) projects.

* Corresponding author.
E-mail address: aksel.elkjaer@ntnu.no (A. Elkjaer).

https://doi.org/10.1016/j.jmapro.2022.04.029
Received 1 December 2021; Received in revised form 18 April 2022; Accepted 22 April 2022
Available online 19 May 2022

growing demand for electric transportation. Aluminum conductors are suited for electric vehicles as weight-saving is essential, and aluminum is often inherent in the electrical design, as aluminum is used as a current collector in popular battery cell technologies [6]. Therefore, aluminum is already present in the electric circuit, and its wider use for connecting battery cells into larger networks and downstream components is beneficial.

Aluminum is a more abundant metal than copper on Earth, resulting in a lower and more stable price [4]. However, the greater difficulty in forming reliable electrical connections inhibits wider adoption. Aluminum's rapidly forming and highly insulating oxide layer, combined with lower strength and greater thermal expansion than copper, complicates contact design [7]. In particular, mechanical compression contacts (e.g. bolted or crimped connections) of aluminum interfaces are susceptible to fretting failure [8]. Fretting of aluminum contacts may cause dramatic increases in resistance as insulating aluminum-oxide particles build up between the contacting interfaces. One method to prevent a fretting failure would be to weld connections, as a welded connection removes the possibility for oxide particles forming between the contact interfaces [7]. A copper compatible welding method would therefore enable aluminum to be utilised more in electrical applications and interface to a wider range of existing components.

Unfortunately, traditional fusion welding is not suited for joining aluminum and copper as the required melting temperatures promote the formation of brittle intermetallic compounds [9]. Instead, lower heat input processes are utilised to reduce the formation of intermetallic compounds while still achieving bonding [9]. Generally, investigations of Al-Cu joints have shown that welds with an intermetallic thickness above 2 μm have significantly degraded structural integrity [10,11]. Low heat input processes, such as friction welding [12–14], cold rolling [11,15–18] and ultrasonic welding [19–21], can join aluminum and copper with intermetallic thicknesses below 2 μm. However, the weld interface may be a source of electrical resistance, provoking a hot spot under operation [12]. High operating temperatures are detrimental to Al-Cu conductors as they accelerate solid-state diffusion, promoting the formation of intermetallic compounds over time. An ideal Al-Cu joining process should form a structural bond with minimal intermetallic compounds, low electrical resistance and a slow diffusion rate, therefore maximising the conductor's operational performance.

In this study, we investigate the performance of Hybrid Metal Extrusion and Bonding (HYB) for joining aluminum and copper. Hybrid Metal Extrusion and Bonding (HYB) is a novel joining process capable of welding along joint lines [22]. The results in this paper provide the first characterisation of the HYB process for electrical applications. The results show that the HYB process forms a thin intermetallic layer with negligible impact on electrical resistance. Artificially ageing the HYB welds by heat treatment caused continued diffusion with the formation of AlCu, Al_2Cu and Al_4Cu_9 in three distinct layers. The intermetallic growth rate was slower than alternative processes, and the intermetallic layers did not increase the electrical resistance. The results indicate that the HYB process is well-suited for joining Al and Cu, providing reliable operation at high temperatures.

2. Methodology

2.1. Manufacturing test specimens

Hybrid Metal Extrusion and Bonding (HYB) is a joining process that uses continuous extrusion of filler material to join offset interfaces [22]. The following section provides an overview of the setup and welding parameters used to manufacture the test specimens in this study. For a complete description of the HYB process and detailed analysis of welding parameters, see Grong et al. [23] and Sandnes [24].

Fig. 1 shows a schematic drawing of the experimental set-up during Al-Cu butt welding. Included in the sketch is the HYB PinPoint extruder with its main tool parts. The extruder is built around a rotating pin with

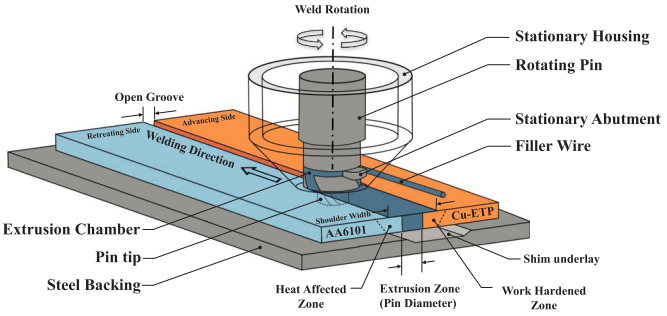

Fig. 1. Schematic illustration of HYB PinPoint extrduer for butt joining Al-Cu. Prior to the joining operation the two base plates are clamped onto a steel backing with a fixed spacing of 4 mm, where the aluminum plate is placed on the retreating side (RS) and the copper plate on the advancing side (AS) of the joint.

a set of moving dies through which the aluminum is allowed to flow. The pin rotates at a constant speed so that the inner extrusion chamber with its three moving walls will drag the aluminum filler wire (FW) both into and through the extruder, due to the imposed friction grip. At the same time, it is kept in place inside the chamber by the stationary housing constituting the fourth wall.

Prior to the butt welding operation, the two base plates are first mounted in a fixture with a fixed spacing of 4 mm. The plates rest on a steel backing. During welding, the HYB PinPoint extruder slides along the joint line at a constant travel speed. At the same time the rotating pin tip (7 mm) with its moving dies is submerged into the groove between the plates to be joined. Because the moving dies extend into the groove, the aluminum will start to flow through them as soon as the filler wire (FW) hits the abutment, and the pressure build-up will become sufficiently large to initiate extrusion. The pin tip is positioned to only touch the copper base metal (Cu-BM) groove wall without actually machining it. In contrast, the aluminum base metal (Al-BM) on the retreating side (RS) of the joint will be dragged along with the rotating pin shoulder (12 mm) and deposited in the groove behind, where bonding with the filler metal (FM) occurs inside the extrusion zone (EZ). By proper pre-setting of the two main process parameters controlling the FM deposition rate (i.e. the FW diameter and the drive spindle rotational speed), the entire groove cross sectional area can be filled in one pass. The welding parameters are listed in Table 1.

The samples were manufactured from a 3 mm rolled AA6101 H19 plate and a 3 mm ETP-Cu bar, using an Ø1.4 mm AA6082 filler wire. The welds in this study were the first time the HYB process had been used to join aluminum and copper in a butt weld configuration. Previously, the HYB process has been used to join aluminum and copper in a state-of-the-art four material (Al-Cu-Ti-Fe) weld [25]. Characterisation of the Al-Cu interface in this weld indicated that having copper on the retreating side increased the likelihood of gaps and deformations occurring [25]. Similarly, Galvao et al. reported that friction-stir butt welds of aluminum and copper generally perform better with copper on the advancing side [3]. Therefore, the welds in this study were performed with copper on the advancing side and aluminum on the retreating side. In addition, two 0.1 mm steel shims were used as an underlay for the weld, having been found to aid the weld formation.

Table 1
Welding parameters used for HYB butt joining Al-Cu.

Open groove (mm)	Pin rotation (RPM)	Welding speed (mm/s)	Wire feed rate(mm/s)	Gross heat input(kJ/mm)
4	350	12	125	0.16

2.2. Test specimen characterisation

The 3 mm thick welded plate was subsequently cut into 2 mm wide strips, with a length of 50 mm (20 mm copper and 30 mm aluminum). Hardness measurements were performed across the weld interface using an HM-220 Mitutoyo Micro-Vickers hardness testing machine. Hardness tests were repeated three times at the same location by grinding the cross-section interface after each repetition. Measurements were performed with 0.5 mm spacing and 1 kgf test load.

One cross-section was ground, polished and leached with an alkaline solution of 1 g NaOH per 100 ml H2O for examination in an Alicona Confocal microscope.

The height of specimens for heat treatment and electrical resistance measurements was reduced from the initial plate thickness of 3 mm to 2 mm. A nominal 0.75 mm was removed from the top and 0.25 mm from the bottom to achieve a planar interface for electrical characterisation.

The specimens were heat-treated at 200 °C and 250 °C in a Heraeus T 5042 EK drying cabinet and at 350 °C in an ESAB PK 410 drying cabinet. Individual specimens were removed at three time intervals with the longest exposure exceeding 1000 h for each temperature.

2.2.1. Electrical characterisation

A custom measurement jig was used to measure the resistance of the test specimens. The jig, illustrated in Fig. 2, provided consistent voltage pickups with 2 mm spacing over a total length of 32 mm. Four-point electrical resistance measurements were performed for each voltage pickup location using a 3 A measurement current. The voltage drop over the complete specimen was monitored for 30 min before starting measurements along the specimen length. The monitoring was performed to confirm negligible self-heating of the specimen and stable performance of the measurement equipment. Measurements were performed with a PeakTech 6135 power supply and Fluke 8864A precision multimeter.

2.2.2. Microstructural characterisation

After measuring the electrical resistance, the sample's microstructure was examined using electron microscopy. A FEI Apreo field emission scanning electron microscope (SEM) operated at acceleration voltages in the range of 10–20 kV, was used to inspect the samples heat-treated at 250 °C and 350 °C. The SEM samples were ground using SiC papers down to a grit size of 2000 and polished using cloths with 3 μm and 1 μm diamond abrasives. Backscattered electron imaging (BSE) and SEM X-ray energy dispersive spectroscopy (EDS) using an Oxford Xmax 80 SDD EDX detector were used to reveal the formation of intermetallic phase layers.

FEI Helios G2 and G4 dual-beam focused ion beam (FIB)-SEMs were used to prepare lamellae from polished joint cross-sections of a non-heat treated, and from joints heat-treated at 200 °C and 250 °C. The lamellae were then inspected using a JEOL JEM 2100 for transmission electron microscopy (TEM), and a JEOL JEM 2100F and a JEOL double corrected JEM-ARM200CF integrated with CEOS spherical aberration correctors for scanning TEM (STEM) imaging, and using an Oxford X-Max 80 SDD EDX and Centurio EDS detector for STEM-EDS. The intermetallic layer thickness was determined by comparing annular dark field (ADF) STEM images with bright field (BF) TEM images and EDS maps. The EDS maps were analysed and visualised using the python library hyperspy [26]. Twenty intermetallic phase (IMP) thickness measurements were done on each sample. Electron diffraction zone axis patterns and precession electron diffraction patterns were acquired to assess possible phases in the observed layers.

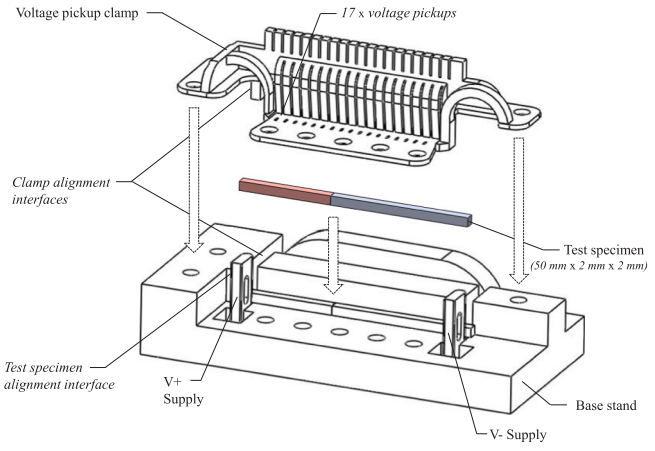

Fig. 2. Electrical measurement jig for four point measurements, comprised of base stand and clamp with 17 voltage pickups.

3. Results

The results are reported in three subsections. In the first section, the initial weld structure (before heat-treatment) is described. Then the results of the heat-treated samples are presented in the second and third sections. The second section presents the electrical performance and the third section presents the microscopy results.

3.1. Initial weld structure

In Fig. 3(a), the Vickers hardness across the interface centreline is plotted with reference to a cross-sectional optical macrograph. The weld cross-section is the original 3 mm plate thickness and was not ground down for heat treatment and electrical resistance measurement. The sample was leached before imaging to contrast the AA6101 base material and the AA6082 filler material. A wide and thin layer of filler material is visible on the top of the weld. The filler material is compressed towards the copper interface before deflecting against the steel underlay at the bottom and spreading further out. The labelled extrusion zone (EZ), consisting of a mix of filler metal and thermomechanically treated aluminum base metal, corresponds to the pin tip diameter of 7 mm.

The hardness measurements show that the base materials properties have been altered outside of the extrusion zone. On the copper side, work hardening has increased the hardness from nominally 108 Hv up to 116 Hv over 2.5 mm. On the aluminum side, a heat affected zone has reduced the hardness from its nominal value of 74 Hv. Inside the extrusion zone, the aluminum hardness averaged 70 Hv over the first 2 mm from the copper interface, before reducing further to 53 Hv. The hardness increased over the remaining extrusion zone but did not recover to the nominal value until outside the heat affect zone.

Fig. 3(b) & (c) shows optical micrographs of the weld interface with increasing magnification. Both images are from the centre of the weld cross-section and show no transfer of material across the interface or mechanical interlocking. A straight interface has been achieved, and intermetallic compounds are not observable under maximum magnification.

Fig. 4a) shows a BF-TEM image of the weld interface in which a continuous intermetallic layer is observable. Diffraction pattern analysis indicates the presence of mainly Al_2Cu and Al_4Cu_9. The average thickness of the intermetallic layer was (0.19 ± 0.01) μm. Fig. 4b) shows an ADF-STEM image from the same sample but different region, along with STEM-EDS element maps (in at.%). Dislocation structures can readily be observed in Cu grains in the ADF micrograph, and has been confirmed using weak-beam dark-field imaging. The yellow rectangle in the micrograph indicates the region from where EDS mapping was done. Two distinct regions may be seen from the element maps, assuming that the TEM sample was successfully made perpendicular to the weld interface. The layer closest to the Al filler material has been found to have an approximate 2:1 ratio of Al and Cu, respectively. The layer closest to the Cu base material was found to consist of an Al and Cu concentration gradient. Another observation from the element mapping is that there seems to be an accumulation of Si and Mg at the IMP layers.

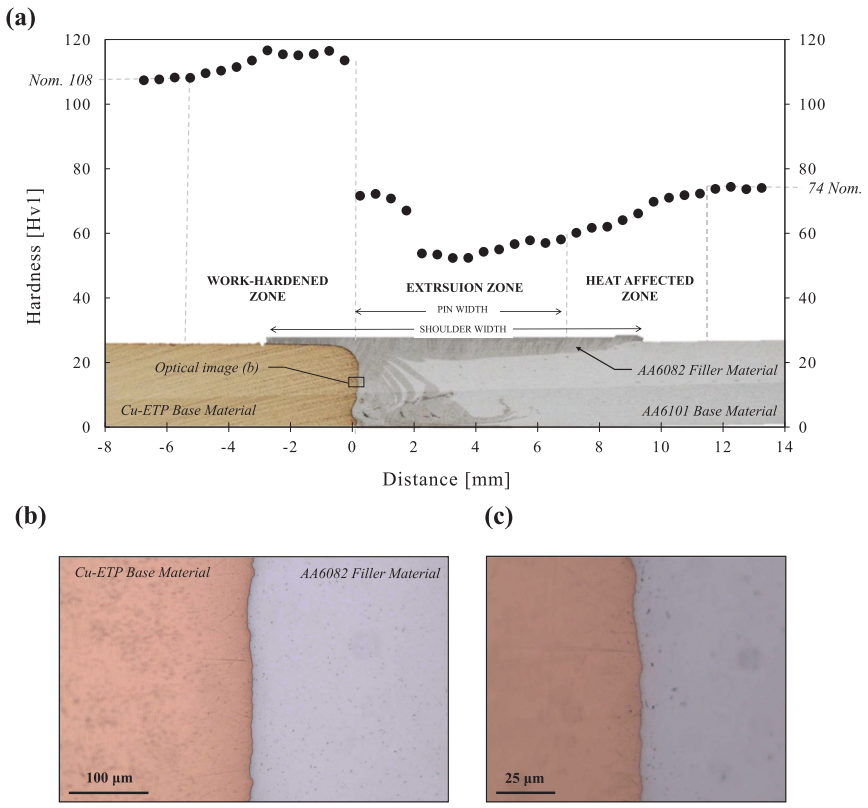

Fig. 3. Initial (without heat treatment) characterisation of 3 mm thick plates joined by HYB process including (a) Vicker hardness measurement across weld interface with reference to leached optical macrograph (b) & (c) higher magnification optical images of weld interface.

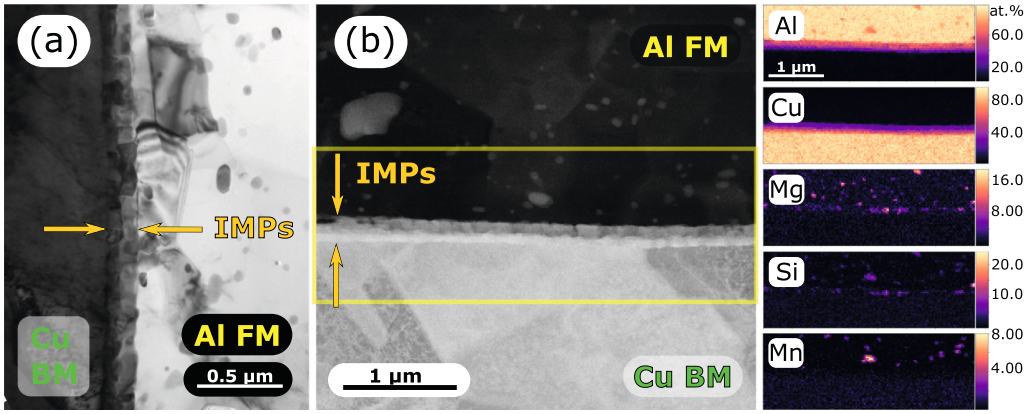

Fig. 4. (a) A bright field TEM image of the Al-Cu interface revealing small nanocrystalline grains constituting a continuous layer between the Cu BM and Al FM. (b) ADF-STEM image from a different region in the same sample. The yellow rectangle indicates the area from where STEM-EDS has been performed (colour bars are in at.%). The EDS element maps indicate the presence of two distinct layers of Al and Cu at the IMP layer: one layer composed of approximately 2:1 ratio of Al and Cu respectively closest to the Al FM, and one region closest to the Cu BM with an Al and Cu concentration gradient. (For interpretation of the references to colour in this figure legend, the reader is referred to the web version of this article.)

3.2. Electrical performance

Fig. 5 show electrical resistance measurements of different test specimens after thermal exposure. The measured resistances have been multiplied by the specimen's cross-sectional area. Hence, the graph's gradient shows the resistivity of each sample. Measurements across the copper are shown in orange and aluminum in blue. Extrapolating the gradient of each material to the interface identifies the interface resistance. In all cases, no significant interface resistance was identified. In fact, the total resistance of all specimens decreased after thermal exposure. The dotted line in each graph (except the 250 °C series) shows the resistance measurement before heat exposure. The gradient of aluminum has decreased relative to the dotted line indicating an increase in the aluminum conductivity. Therefore, as the interface resistance did not increase and the aluminum's resistivity decreased, the joint's overall resistance has decreased.

The AA6101 H19 base material and AA6082 filler material are both heat-sensitive aluminum alloys, and both alloys had undergone cold working before joining. The AA6101 had been rolled for maximum strain hardening to H19 condition, and the AA6082 had been cold drawn into a wire. Therefore, a reduction in strength and increase in conductivity is expected as the heat treatment would reduce the dislocation density. To quantify the conductivity increase, the conductivity of both base and filler materials were measured before and after 528 h exposure at 350 °C. The conductivity was measured using monometallic test specimens of Cu-ETP and AA6101, while for the AA6082, a 1 m

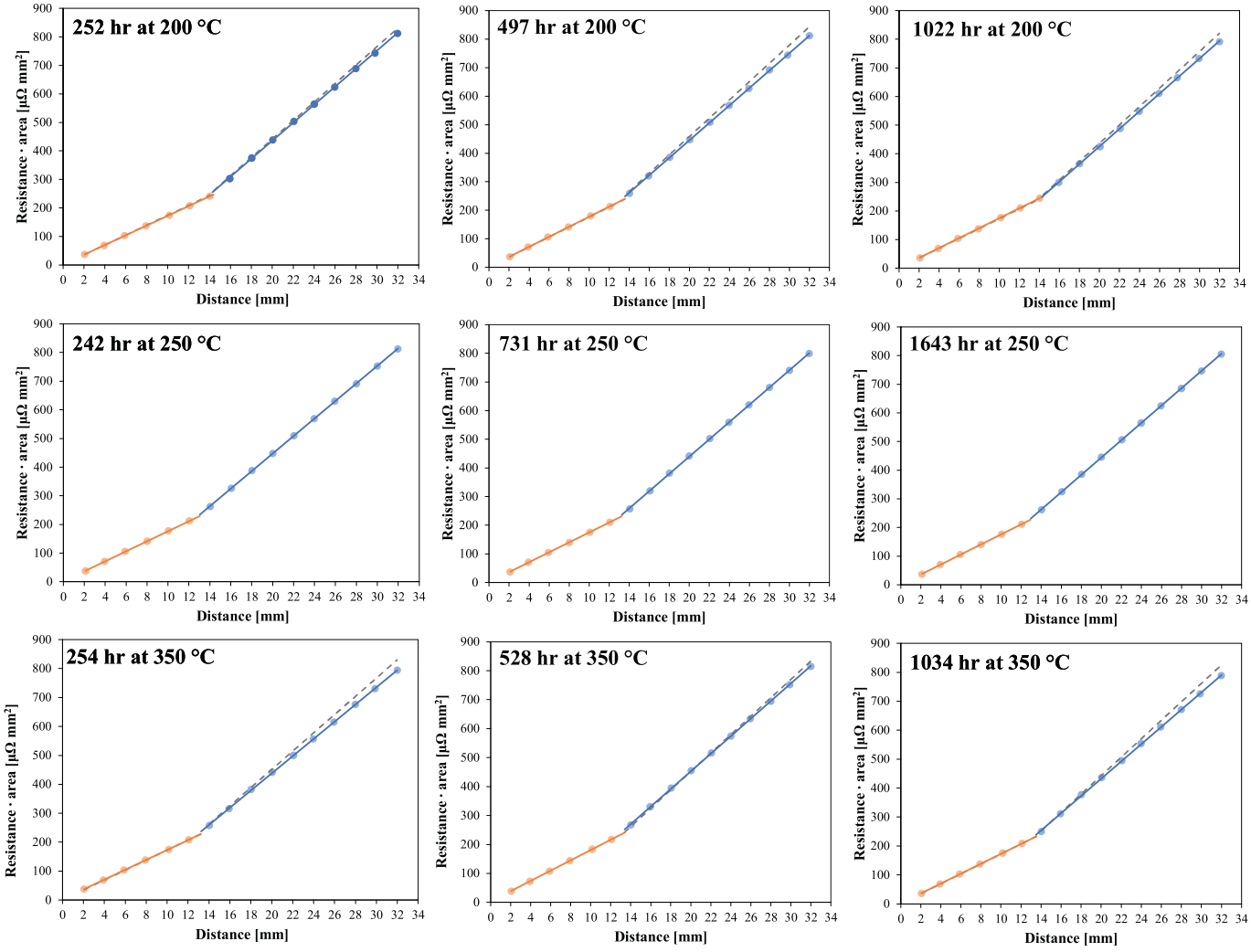

Fig. 5. Resistance measurements of samples heat-treated for increasing durations at 200 °C, 250 °C & 350 °C. Extrapolating resistance measurements to the interface of each sample (between 12 mm and 14 mm) shows the interface causes negligible resistance increase in all cases.

length of wire was measured. The measured conductivity before and after heat treatment is shown in Fig. 6. The AA6082 filler wire showed the greatest increase in conductivity; however, it is expected that the conductivity of the filler wire will increase during the extruding process due to the thermal and mechanical loads.

3.3. Microscopy inspection of heat treated samples

TEM samples taken from three heat treated joints at 200 °C and one at 250 °C were inspected. Fig. 7 shows bright-field TEM images of the maximum exposure 200 °C and 250 °C specimens. It can be seen that the heat treatment has caused Al and/or Cu interdiffusion to take place, giving positive conditions for intermetallic grain growth into a continuous layer.

All the samples studied using TEM have been observed with IMP grains that constitute a continuous layer with a wavy morphology. Some of the samples were also observed with voids both close to the IMP layers and in the Cu-BM a few micrometres away from the Al-Cu interface. The IMP layer of the non-heat treated sample and the specimen annealed at 200 °C for 252 h have a less rough IMP morphology compared with the samples heat-treated for 497 and 1022 h. A crack was discovered on the 1022 h sample on the interface IMP interface to the Cu-BM. TEM was also used to assess the chemical compositions and crystal structures of the grown phases in the heat-treated samples using STEM-EDS and electron diffraction techniques. The results were similar to the features obtained from the non-heat treated sample analysis with the presence of mainly Al_2Cu and Al_4Cu_9. Another observation of the heat-treated samples is that both the Al FM and Cu BM grains contain complex dislocation structures after annealing.

The samples heat-treated at 350 °C were inspected using SEM, as intermetallic phases were observable using light microscopy. Fig. 8 shows BSE images and EDS concentration line profiles across the interface of two materials heat-treated at 350 °C for 254 and 1034 h, respectively. The images and profiles show three distinct layers of intermetallic phases, and indicate the presence of the previously identified Al_2Cu (θ) and Al_4Cu_9 (γ_1), as well as the frequently reported AlCu (η) [12,13]. Several delimitation cracks were discovered in the 1034 h sample and occurred along the boundary of Al and the nearby IMP layer, as labelled in Fig. 8(b).

The mean values and corresponding standard deviation of the intermetallic thicknesses measured for each thermal exposure are shown in Table 2. The inspection method is specified in the table footnote.

4. Discussion

4.1. Electrical performance

A primary finding from characterisation of the Al-Cu HYB weld is the

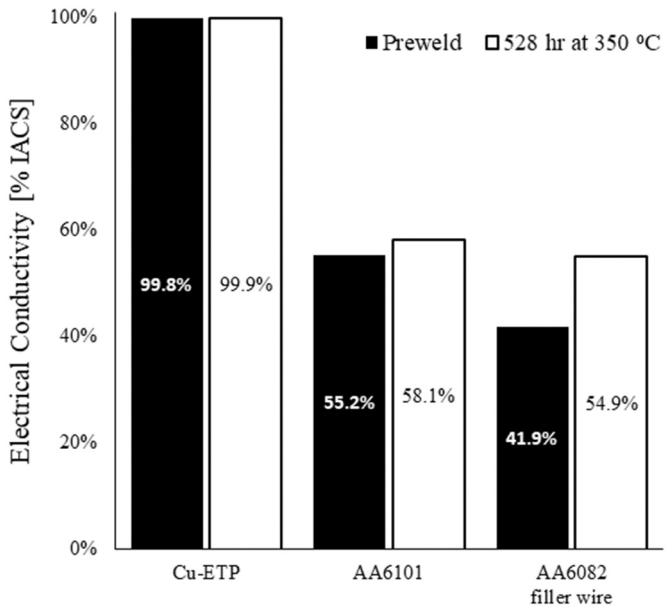

Fig. 6. Bulk conductivity measurements of weld materials before and after heat treatment at 350 °C for 528 h.

absence of increased electrical resistance. A critical concern for bimetallic busbars is increasing electrical resistance due to the growth of intermetallic compounds [7]. Previous studies have demonstrated that Al-Cu bimetallic welds have high resistance that can increase further from relatively short term exposure to temperatures above 150 °C [11,12]. On the other hand, the tested HYB welds in this study maintained low resistance even after a maximum thermal exposure of 1034 h at 350 °C. These results contrast the high thermal sensitivity of aluminum copper joining methods reported previously [11,12,27]. Newer studies have achieved the joining of aluminum and copper without increased electrical resistance [28–30]. However, subsequent thermal sensitivity has not been measured and remains identified as a potential risk. The low resistance and temperature stability of the HYB welds indicates good suitability for use in conductors, offering operation at higher temperatures and longer duration than alternative joining processes.

In the following section, the electrical performance of the HYB joint is compared to alternative processes. The comparison shows that the electrical resistance of HYB welds is the least heat-sensitive welds in published literature to the authors' knowledge.

4.1.1. *Electrical performance metrics of bimetallic weld interfaces*

Comparing Al-Cu joining processes is difficult due to variations in test methodology. The most common practice employs four-point resistance measurements [11–14,28–35], while in some cases (typically thin sheets) an eddy current resistivity measurement technique is used [18,36]. Focusing on the more accurate four-point methodology, the difficulty of comparing performance arises from variations in joint configurations and test specimen geometry.

To compare the HYB results to the alternative processes, we first review the frequently reported performance metrics before proposing a new metric, weld interface resistivity, for comparing and evaluating butt welded joint configurations.

Frequently reported electrical performance metrics of bimetallic welds are:

1. Comparison of measured joint conductivity to theoretical conductivity [11–14,28–32],
2. Joint performance factor [30,33–35]
3. Relative resistance increase [11,12].

All such metrics are useful when comparing results with the same geometry. However, they remain, in part, specific to the tested specimen geometry and are not suited for direct comparison across different studies.

The most popular performance metric is joint conductivity. An idealised schematic of the four-point measurement method to measure joint conductivity is shown in Fig. 9. Measuring the voltage drop across the joint, V_J, and current, I, allows the joint resistance, R_J, to be calculated from Ohm's law, Eq. (1). The joint conductivity or its inverse joint resistivity, ρ_J, can then be calculated from the cross-sectional area, A, and measurement length, L as shown in Eq. (2).

$$R_J = \frac{V_J}{I} \tag{1}$$

$$\rho_J = \frac{R_J A}{L} \tag{2}$$

The measured joint resistivity is then compared to the theoretical joint resistivity, ρ_T. The theoretical joint resistivity is determined by calculating the expected joint resistance, R_T, based on the volume-metric ratio of materials in the joint. Calculation of the theoretical resistance is

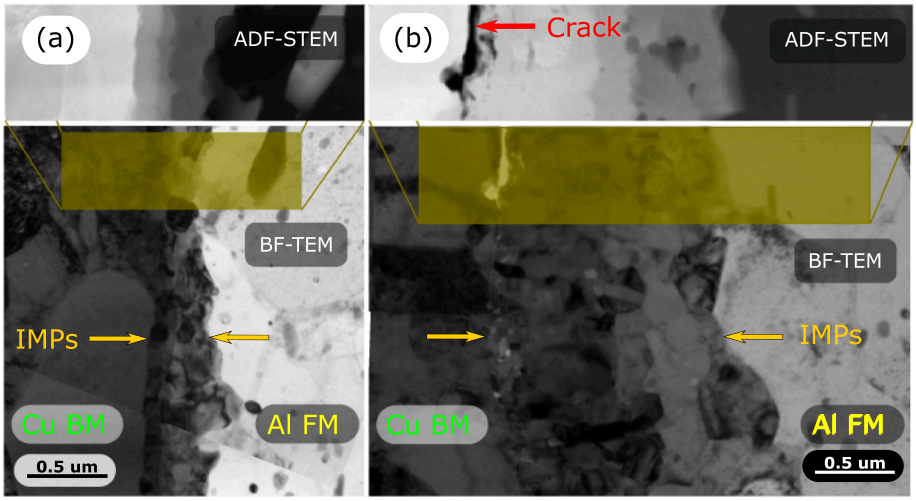

Fig. 7. (a) and (b) show BF-TEM micrographs of heat-treated samples at 200 °C and 250 °C after maximum thermal exposure, revealing growth of IMPs compared with the non-heat treated specimen.

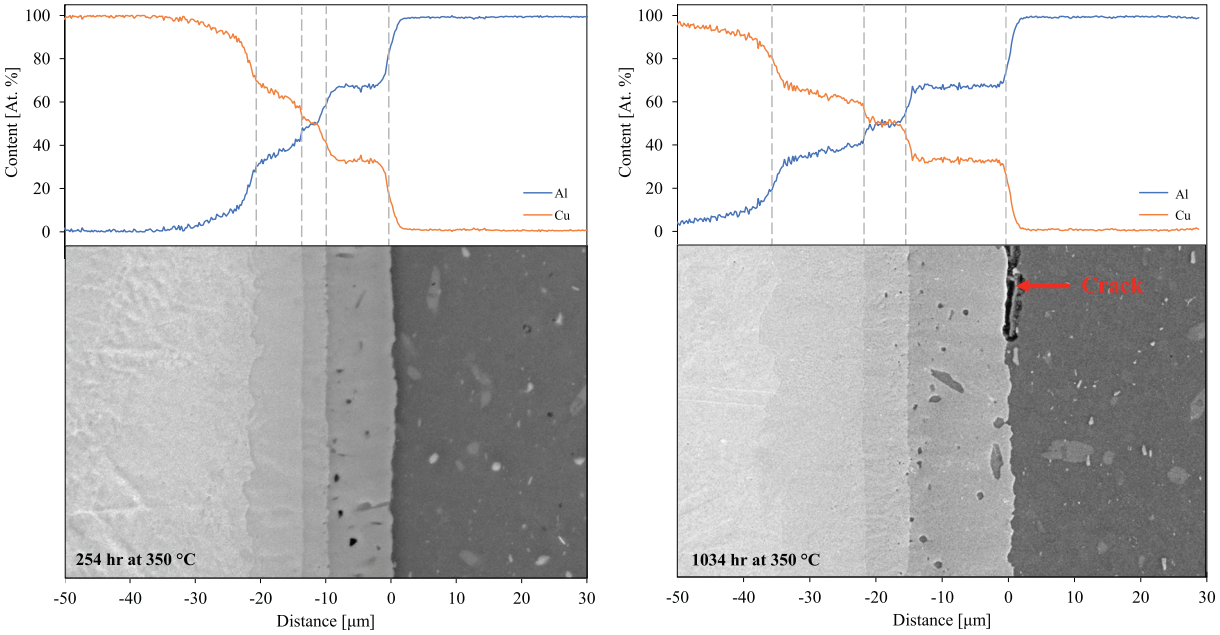

Fig. 8. (a) and (b) show BSE SEM-images and SEM-EDS concentration profiles of Al and Cu across the interface of heat-treated specimens at 350 °C for 254 and 1034 h, respectively.

Table 2
Measured total thickness of intermetallic phase layer after thermal exposure of 200 °C, 250 °C and 350 °C for increasing durations.

200 °C		250 °C		350 °C	
Time [hr]	Thickness [μm]	Time [hr]	Thickness [μm]	Time [hr]	Thickness [μm]
252[a]	0.17 ± 0.02	242[b]	0.84 ± 0.1	254[b]	21.4 ± 0.7
497[a]	0.29 ± 0.06	430[b]	0.88 ± 0.22	528[b]	31.4 ± 0.8
1022[a]	0.36 ± 0.04	731[b]	1.44 ± 0.22	1034[b]	34.9 ± 0.7
		1643[a]	1.63 ± 0.25		

[a] Total intermetallic thickness measured using TEM ADF-STEM images.
[b] Total intermetallic thickness measured using SEM BSE images.

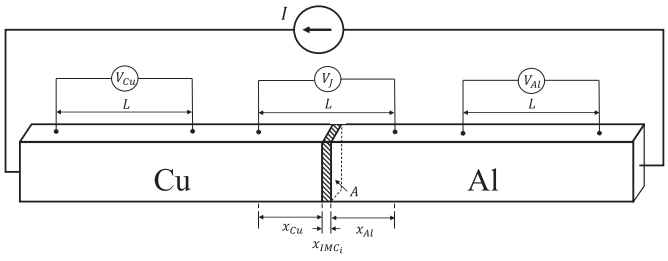

Fig. 9. Illustration of four point electrical measurement method for measuring joint conductivity and joint performance factor.

shown in Eq. (3) where measurement distance, L, illustrated in Fig. 9, is composed of copper length x_{Cu}, aluminum length x_{Al} and intermetallic thicknesses x_{IMC_i}. The theoretical joint resistivity is then calculated from the joint resistance as shown in Eq. (4).

$$R_T = \frac{1}{A}\left(\rho_{Cu}x_{Cu} + \rho_{Al}x_{Al} + \sum \rho_{IMC_i}x_{IMC_i}\right) \tag{3}$$

$$\rho_T = \frac{R_T A}{L} \tag{4}$$

In most cases, the volume-metric ratio of sample being measured is 50% Al: 50% Cu and the contribution of intermetallic compounds is neglected from the theoretical resistance. The quality of the joint is then assessed by how close the measured resistivity is to the theoretical resistivity. A quality metric, ε, may be defined to quantify the difference, Eq. (5), but in most cases results are compared graphically. Comparison of conductivity is both intuitive and practical yet conceals a few limitations for comparison between different studies.

$$\varepsilon = \rho_J - \rho_T \tag{5}$$

The first limitation is the importance of measurement length. For example, the perceived quality of the same joint can be increased by increasing the measuring length. Increasing the measurement length increases the joint conductivity as the relative contribution of the interface resistance is reduced. Therefore, a direct comparison of joint conductivity is only valid when comparing the same measurement length.

A second limitation when comparing to theoretical conductivity is the difficulty in controlling the volume-metric ratio of base materials in the test specimen. From the first limitation, it follows that measurement length should be minimised to maximise the contribution of interface resistance (i.e. minimise bulk resistance from the measurement). However, when measuring over shorter distances, controlling the volume-metric ratio becomes more challenging as the distance to the interface on each material side becomes smaller. For example, when the measuring distance is 10 mm, a deviation of 0.5 mm changes the ratio of base materials to 55%: 45%. Then, when comparing the measurements to a theoretical value of 50%: 50%, the perceived interface resistance will be higher for 55% Al or lower if 55% Cu. In some studies, the reported joint resistance is below the theoretical resistance, indicating that copper's volume-metric ratio in the measurement has not been suitably controlled [29,30]. Eslami et al. [30] highlighted the difficulty in achieving a consistent volume-metric ratio due to the non-uniform distribution of Al and Cu achieved in their friction-stir welded test specimens.

A third limitation when assessing conductivity is the need to compensate for, and potential inaccuracies in, bulk connectivity. The conductivity of aluminum and copper varies substantially due to alloying and manufacturing treatments. Reported material conductivity in the reviewed studies ranged from 48 to 63% IACS for Al and 82 to 105% IACS for Cu. Several studies did not specify if bulk conductivity was

measured [11,12,28], and in a few studies it was not measured [30], or reported [13]. Accurate characterisation of bulk conductivity is important for assessing the joint conductivity and establishing the interface's contribution to resistance.

One method to suitably compensate for the bulk conductivity is to measure and report the joint performance factor, k. The joint performance factor is calculated by comparing the resistance of the joint to equivalent measurements of both bulk materials, Eq. 6. In this case, the voltage drop across the copper, V_{Cu}, and aluminum, V_{Al}, is measured over the same length, L, as the joint, see Fig. 9. Joint performance factor is suited for evaluating overlap joints as a meaningful length is established from the overlap distance. However, the joint performance factor of a butt joint relies on an arbitrary measurement length. Therefore, as different studies use different measurement lengths a direct comparison is not possible, and the metric is still susceptible to an erroneous volumetric ratio.

$$k = \frac{2V_J}{V_{Cu}V_{Al}} \tag{6}$$

The last typically reported performance metric is relative resistance increase and is useful in capturing the effect of heat treatment. This metric differs from the conductivity and joint performance factor assessment, as it does not assess the manufacturing quality but rather degradation from further environmental exposure. Eslami et al. [30] pointed out that most studies on friction stir Al-Cu welds focus on process parameters and not on subsequent functional testing of welds. As such, most studies have not performed heat treatment ageing and this metric was only identified in a few studies [11,12]. The metric effectively captures weld degradation. However, it is poorly suited for comparison across different studies. The starting resistance is specific to specimen geometry and therefore requires normalisation of measurement length and area for comparison, and to identify the weld interface resistance.

4.1.2. Weld interface resistivity

After reviewing previous studies on the electrical performance of Al-Cu joints, we propose using a new metric, weld interface resistivity, η ($\mu\Omega$ mm^2), for the electrical assessment of welds. Measurement of weld interface resistivity is analogous to the measurement of electrical or thermal contacts. In such domains, the performance metrics, specific contact resistivity ($\mu\Omega$ mm^2) [37], and thermal contact resistance, (K W^{-1} mm^{-2}) [38], are used to quantify the interface resistance. In both contexts, the interface resistance occurs over a very short distance and is normalised only for the cross-sectional area. Therefore, the bulk electrical or thermal resistances are excluded from the measurement allowing direct comparison to other processes. To exclude the bulk contribution from the measurement, several measurements are made on either side of the interface and extrapolated to the interfaces (as shown in Fig. 5).

Weld interface resistivity is an ideal metric for evaluating bimetallic materials as it envelopes multiple performance aspects. Several studies that measured the electrical resistance across weld interfaces have shown that the resistance increase cannot be attributed solely to the higher resistivity of the intermetallic compounds present in the weld [11–13,29]. Pfeifer et al. [39] have measured the resistance of individual Al_xCu_y intermetallic compounds, and shown they can be up to 11 times the resistivity of copper. However, when calculating the expected resistance across a weld interface, using the individual resistivity measurements and measured thicknesses of intermetallic phases, the measured resistance is even greater than predicted [11–13,29].

Braunovic & Alexandrov [12] suggest possible explanations for the increased resistance as porosity, cracking, changes in grain sizes, and increased dislocation density across the interface. Wang et al. [29] proposed a mechanism for the non-linear increase in resistance by relating intermetallic thickness to the base materials' grain sizes, as well as possible contributions from cracks, oxides and residual stresses. Traditionally, the criteria for acceptable Al-Cu bimetallic joints have been based on intermetallic thickness alone. However, consideration of thickness alone neglects the potential differences in joining processes and their non-linear contributions to resistance. The proposed properties by Wang and Braunovic & Alexandrov are influenced by the chosen joining process and its parameters. Therefore, it is not only the intermetallic thickness which determines the performance of the weld but the process and resulting weld structure. Wang et al.'s [29] results exemplify the importance of the process and weld structure over intermetallic thickness measurements alone, as they reported a diffusion brazed joint with 50 μm total intermetallic thickness that had a lower resistance than a flash welded joint with 2 μm total intermetallic thickness.

In contrast to intermetallic thickness, the weld interface resistivity metric captures process dependent factors, combining the intermetallic compounds resistivities, working length and structural defects into a single metric. Combining both resistivity and total intermetallic thickness into one measurable metric allows different processes to be directly compared. Furthermore, the metric is practical allowing comparison to bulk properties and functional performance for given geometric applications.

The weld interface resistivity has been calculated for several existing processes and compared to HYB performance in Fig. 10. The weld interface resistivity has been calculated for existing process from previous studies using the bulk conductivity and specified measurement distances. The calculation equations are shown in Eq. (7), and the input and result for each study is shown in Table 3. In each study, the best case, lowest resistance, has been used for comparison. For HYB, a value of <10 $\mu\Omega$ mm^2 has been considered, using the previously mentioned and more accurate methodology of forecasting multiple measurements, see Fig. 5.

$$\eta = AR_J - (\rho_{Cu}x_{Cu} + \rho_{Al}x_{Al}) \tag{7}$$

The comparison of weld interface resistivity in Fig. 10 is split into two groups, pre and post heat-treatment. The HYB joint is the only study in which the interface resistance is negligible in both groups. The HYB joint weld interface resistivity is comparable to the best friction-stir welded results of Eslami et al. [30] however Eslami et al. did not perform measurements after heat treatment. Garcia-Navarro et al. [40] recently highlighted that there is limited information on the electrical performance of friction stir weld. Therefore, it is worth highlighting that Fig. 10 shows several studies have reported lower electrical resistance of friction welds since the highly cited Braunovic & Alexandrov [12] characterisation.

The majority of studies on Al-Cu welds has focused on welding process parameters and have not measured artificially aged samples. Therefore, fewer results of samples post heat-treatment are reported. However, those that measured heat treated samples all showed increased resistance. Calculation of the weld interface resistivity for Wang et al.'s [29] diffusion brazed specimens is negative as Wang et al. reported a joint resistivity below the theoretical for the base materials. Wang et al. highlighted the “abnormal” results, and while the result indicates potential inaccuracy in measurement distance or bulk conductivity; we included the measurement as it provides another example of increased resistance from thermal exposure.

It is not appropriate to compare the weld interface resistivity increases from each study, as the samples were heat-treated at different temperatures and duration in each study, as specified in Table 3. Nevertheless, Table 3 shows the HYB samples thermal exposure was greater than the other studies and still did not increase in electrical resistivity. The HYB process has therefore formed a weld structure without added resistance and remained stable over the tested temperature range; indicating a conductor using a HYB joint could operate for longer, and at higher temperatures, compared to alternative joining processes.

4.1.3. Sample geometry resistance

The HYB joining process also provides the ability to further reduce

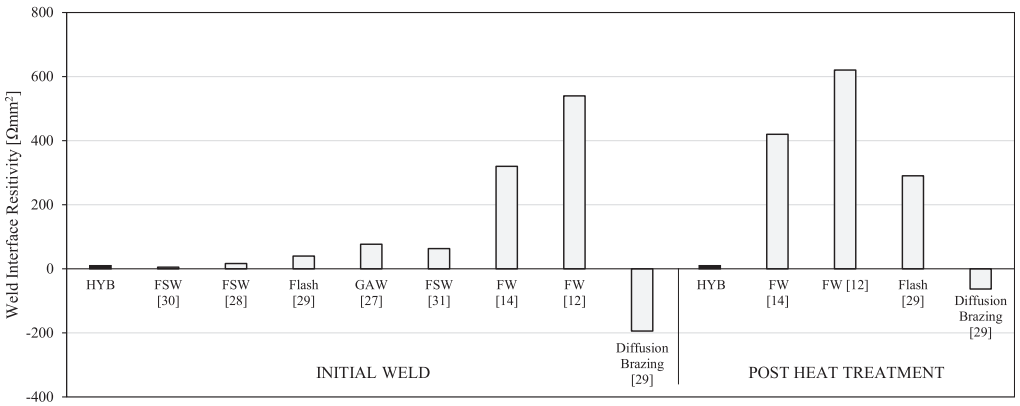

Fig. 10. Comparison of weld interface resistivity for different Al-Cu joining processes calculated from previous studies and compared to HYB results.

the weld interface resistance versus the reported measurements. The test specimens for resistance measurements were cut and ground into 2 mm × 2 mm × 50 mm samples to form a planar interface, see Fig. 11. However, the use of a rotating pin with 3 mm shoulder increases the weld interface area over the top of the copper as shown in Fig. 12. The weld interface area of 6 mm 2 per mm for a plate thickness of 3 mm provides a conductor area to weld interface area ratio of 2, whereas, the resistance measurement sample had a ratio of 1. Increasing the ratio of conductor area to weld interface area further reduces the interface resistance. Furthermore, the HYB process can be modified to extrude a weld reinforcement on top of the interface during joining, also shown in Fig. 12. A weld reinforcement would increase the cross-sectional area of the conductor therefore reducing the resistance locally. The local decrease in resistance would ensure the weld's operating temperature was lower than the nominal conductor temperature.

4.2. Intermetallic growth rate

Isothermal growth of intermetallic compounds in bimetallic materials typically follows a parabolic time law [41]. As such, the intermetallic thickness can be expressed by the equation $y = kt^n$, where, y, is the thickness, k, diffusion rate constant, t, reaction time, and, n, is the time exponent.

To assess the intermetallic growth rate of the HYB joints, the reported results in Table 2 are plotted on the log-log graph shown in Fig. 13. A log transformation of the parabolic equation provides a linear representation of the growth rate, n, as $\ln y = n \ln t + \ln k$. Kidson [41] showed by using Fick's first law of diffusion that a reaction rate controlled by volume-metric diffusion has a time exponent of 0.5. Fig. 13 shows the linear regression for each of the tested temperatures indicating volume-metric diffusion was occurring. The time exponents ranged from 0.35 to 0.55, and Gueydan et al. [42] reported a tolerance of 0.5 ∓ 0.1 as typical for bulk diffusion.

Assuming volume-metric diffusion; the intermetallic growth equation can be considered as $y^2 = k^2 t$ across the tested temperature range, and the diffusion rate constant can be predicted by the Arrhenius equation as follows:

$$lnk^2 = lnk_0^2 - \frac{Q}{RT} \tag{8}$$

Eq. (8) is only dependent on temperature, T, with the pre-exponential factor, k_0, growth activation energy, Q, and gas constant, R, all in principle constant.

Plotting the diffusion constants for each temperature on an Arrhenius plot, Fig. 14, shows a linear diffusion rate increase over the tested temperature range. From the linear regression, an activation energy of 152 kJ/mol and a pre-exponential constant of 1.2E−3 m^2/s can be used to describe the diffusion rate constant of the HYB welds.

4.3. Comparison of growth rate with alternative processes

The activation energy and pre-exponential constant for aluminum and copper interfaces have been reported for several processes [11–21,42–46]. A summary of the diffusion properties from each study is shown in Table 4.

The table shows the tested temperature range and duration applicable to the calculation of activation energy. In some cases the pre-exponential was not reported. Such cases are identified in the table and have therefore been calculated based on the provided measurements. Correct calculation of the pre-exponential was checked by confirming the reported activation energy was correctly calculated.

A widely used criterion for the integrity of Al-Cu welds is maintaining a total thickness of intermetallic compounds below 2 μm [11,12,31,40,47,48]. Therefore, it is interesting to quantify the operational conditions (temperature and duration) that a weld can tolerate before reaching 2 μm. Fig. 15 shows the time taken for the growth of 2 μm at 200 °C.

The calculated duration of the HYB weld to reach 2 μm is an order of magnitude greater than results from alternative processes. We chose to show performance at 200 °C as it is an important operating condition that has previously limited the utility of welded Al-Cu conductors [12]. Typically, maximum operating temperatures for conductors are 130 °C, and at nominal temperatures of 70 °C intermetallic growth is acceptable with existing processes [48]. However, Kemsies et al. [49] have highlighted a trend for higher operating temperatures, and Braunovic [12] has pointed out that temperatures of 200 °C and higher often occur in network overload conditions. Similarly, Gueydan et al. stated that local temperature of Al-Cu conductors in automotive applications may reach 200 °C. Therefore, a weld that can tolerate operation at 200 °C provides increased reliability for a realistic design condition. Fig. 15 shows that both friction welding and cold rolling are susceptible to failure from a relatively short duration at 200 °C temperatures, whereas the HYB process has a greater safety margin for such high-temperature events.

It should also be noted in Fig. 15 that the calculated durations are for 2 μm growth and exclude the starting thickness. An indication of the applicable starting thickness is shown in Table 4. However, in some case the initial thickness is not measured and therefore the first thickness, from shortest thermal exposure, is reported. The HYB weld starting thickness of 0.2 μm is at the lower range of reported value and therefore will not significantly reduce the calculated time to 2 μm in Fig. 15.

A detailed explanation for the thin intermetallic region and high activation energy achieved by the HYB process is beyond the scope of this work. However, the novel process conditions and resulting weld structure, with nanocrystalline interface shown in Fig. 4, contain several unique features compared to alternative processes.

In particular, the use of filler material in a solid-state process is unique to the HYB process. Compared to friction stir welding, the

Table 3
Calculation and comparison of specific interface resistivity from previous studies.

Source	Process	Aged condition	Specimen dimensions [mm × mm^2]	Base material	[% IACS]	Base material	[% IACS]	Theoretical resistance [μΩ]	Measured conductivity [% IACS]	Measured resistance [μΩ]	Interface resistance [μΩ]	Specific interface resistivity [μΩ mm^2]
	HYB	Initial weld		AA6101	55.2%	ETP-Cu	99.8%			164.9		<25
Fig. 5	HYB	1000 h at 350 °C	32 × 4	AA6101	55.2%	ETP-Cu	99.8%			161		<25
Zhang et al. (2020)	GAW	Initial weld	100 × 30	AA1060	60.7%	T2 Cu	104.7%	112.2	74%	116.0	3.8	76.7
	Flash	Initial weld							75%	9.2	0.2	40
Wang et al. (2020)	Diffusion	350 °C 500 h	100 × 250	AA1060	60.5%	C11000	104.5%	9.0	68%	10.2	1.2	290
	Brazing	Initial weld							84%	8.2	−0.8	−194
		350 °C 500 h							79%	8.7	−0.3	−63
Braunovic & Alexandrov (1994)	FW	Initial weld	100 × 75.5	Al	50.7%	Cu	86.2%	137.5	53%	165	27.5	540
		325 °C 120 h (Oven)		Al	50.7%	Cu	86.2%	137.5	52%	169	31.6	620
Li et al. (2018)	FW	Initial weld	10 × 28	AA1060	49.3%	T2 Cu	82.1%	10.0	29%	21.4	11.4	320
		400 °C 2 h		AA1060	49.3%	T2 Cu	82.1%	10.0	25%	25.0	15.0	420
Savolainen et al. (2006)	FSW	Initial weld	99 × 160	EN AW-6060 T6	47.8%	Cu-OF	84.1%	17.5	60%	17.9	0.395	63.2
Eslami et al. (2019)	FSW	Initial weld	40 × 80	EN AW-1050A	59.5%	EN CW008A	98.5%	11.6	75%	11.46	−0.2	<5
Olafsson et al. (2020) & Olafsson (2017)	FSW	Initial weld	24 × 30	AA1050	57.5%	Cu OF 04	95.3%	19.2	84%	19.8	0.55	17

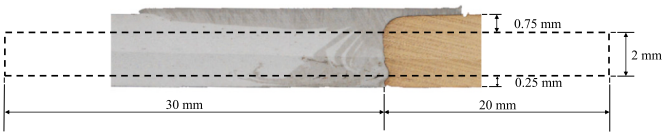

Fig. 11. Dimensions of resistance measurement test specimen with reference to weld cross-section showing the 3 mm plate thickness was reduced to 2 mm.

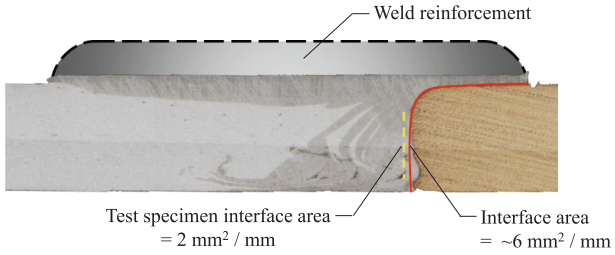

Fig. 12. Illustration of reinforced weld and weld interface area highlighted. Highlighted area shows as manufactured weld interface area (red) and weld interface area (yellow) of resistance measurement test specimen. (For interpretation of the references to colour in this figure legend, the reader is referred to the web version of this article.)

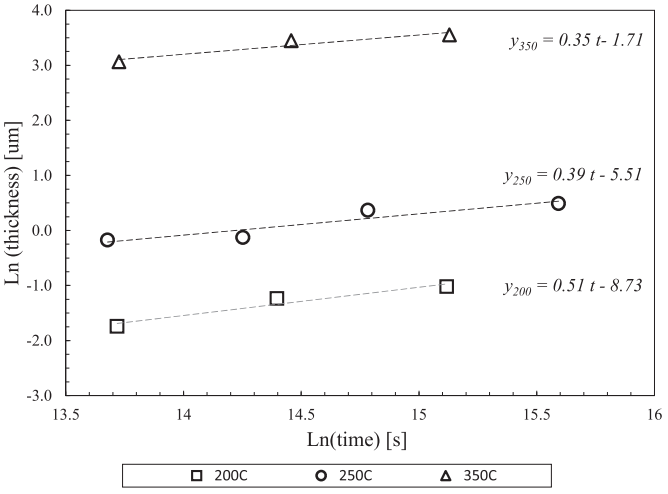

Fig. 13. Loglog plot of intermetallic thickness measurements at 200 °C, 250 °C & 350 °C.

interface temperatures are reduced by machining with lower rotations speeds and not cutting into the harder copper material. Therefore, using a filler material likely provides a less concentrated heat input at the interface than friction stir.

While the primary factors for the formation of intermetallics are temperature and exposure time; the weld microstructure properties may also impact diffusion rate. Hua et al. [16] have modelled the growth of intermetallic and shown that prediction of diffusion rates is improved by considering the unique concentration gradients across the weld. Their findings indicate that the weld structure (i.e. the number of intermetallic compounds and constituent elements present along with the relative thickness ratios of the layers) will impact the overall diffusion rate.

Fundamentally, a slow diffusion rate indicates a reduced density of vacancies across the HYB weld. Diffusion between two metals is dependent on atoms moving into vacancies in the opposite lattice structure [20]. The number of vacancies is influenced by microstructure properties, including dislocations, grain boundaries and defects, which are dependent on the joining process's thermomechanical conditions.

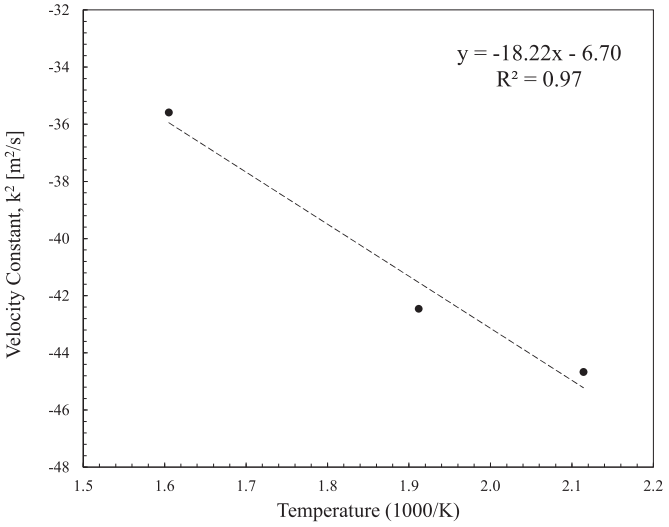

Fig. 14. Arrhenius plot of intermetallic growth rates at 200 °C, 250 °C & 350 °C.

Hence, the HYB results are a unique function of the process temperature profile, resulting intermetallic compounds present and susceptibility to generating vacancies.

5. Conclusion

This study evaluated the Hybrid Metal and Extrusion Bonding (HYB) process for joining copper and aluminum. The main findings were:

- The two materials were joined successfully. Optical examination of weld cross-sections showed a straight interface with minimal material transfer. Transmission electron microscopy identified a thin (0.2 μm) and consistent intermetallic layer had been achieved.
- Weld samples were artificially aged by heat treatment and examined under further electron microscopy to identify intermetallic compound growth. Diffraction pattern analysis indicated the presence of Al_2Cu (θ) and Al_4Cu_9 (γ_2) intermetallic phases. Composition analysis of samples exposed to the highest temperature also indicated presence of AlCu.
- The calculated activation energy for total intermetallic growth was higher than existing processes, including friction welding, cold rolling, and ultrasonic wire bonding, meaning that the intermetallic growth rate is lower for HYB welds.
- The weld interface was not a source of additional resistance, and heat-treated samples did not increase electrical resistance. A new metric, weld interface resistivity, was proposed for the comparison of weld resistance between different processes. The heat-treated HYB samples were found to have the lowest interface resistance of any Al-Cu joining process to the authors' knowledge.

HYB is a versatile joining method capable of joining bulk materials along joint lines. The HYB process allows the joining of larger conductors than possible with ultrasonic welding, and provides greater dimensional flexibility than cold rolling or rotary friction welding. The process is comparable to friction-stir welding; however, HYB forms an interface with significantly less material transfer and less impact on electrical resistance than previously reported for friction stir. Therefore, the novel HYB process shows excellent potential for joining aluminum and copper. This study is the first assessment of the HYB process for bimetallic electrical conductors prompting exciting opportunities for further development.

Table 4
Summary of Al-Cu bimetallic diffusion properties reported using different joining processes in previous studies.

Reference	Year	Author	Process	Initial IMC thickness [μm]	Thermal exposure before initial measurement	Temperature range [C]	Max duration [hr]	Heating method	K_0^2 [m^2/s]	Q_d [kJ/mol]
		Elkjaer et al.	HYB	0.2		200–350	1152	Oven	1.2E−03	151.6
[12]						250–380	120	Oven	2.2E−10	72.0
Oven	1994	Braunovic & Alexandrov	FW	<0.3	1 h at 200C	425–520			8.0E−05	136.9
[12]						200–350	24	Electric current	5.9E−11	55.3
Electric						400–500			3.3E−06	110.9
[13]	2005	Lee et al.	FW	<2		300–500	36	Oven	2.1E−06	110.6
[43]	2015	Xue et al.	FSW	~1		250,400	144	Oven	3.9E−05	125.5
[14]	2018	Li et al. &	FW	0.8		400–500	8	Oven	1.5E−05[a]	121.4
[44]	2018	Pan et al.								
[11]	2001	Abbasi et al.	Cold rolled	<0.3	5 h at 250C	250	1000	Oven	na	na
[15]	2007	Chen & Hwang	Cold rolled	~0		300–540	2	Oven	3.1E−06[a]	107.9
[17]	2014	Hilz et al.	Cold rolled	<1		200–400	1000	Oven	2.7E−07	99.0
[16]	2020	Hua et al.	Cold rolled	1.88		320–400	0.4	Oven	–	–
[18]	2020	Li et al.	Cold rolled	<1.3	0.5 h at 300C	300–450	4	Oven	1.1E−05	108.0
[42]	2014	Gueydan et al.	Clad wire	~0		200–300	48	Oven	–	106.0
[19]	2003	Kim et al.	Wire bonding	~0		150–300	250	Oven	4.7E−07	108.9
[20]	2010	Xu et al.	Wire bonding	0.03		200–300	2904	Oven	1.1E−07	97.0
[21]	2019	Liu et al.	Wire bonding	0.2		150–250	3000	Oven	4.6E−11[a]	76.1
[45]	2011	Guo et al.	Diffusion	<5	10 min at 300C	400–500	0.5	Electric current	4.5E−08[a]	80.8
						200–500	120	Oven	4.8E−08	90.3
[46]	2014	Solchenbach et al.	Laser	<2.5	1 h at 200C	50–350	24	Electric current	–	–

[a] Pre-exponential not reported in study. Value has been calculated based on the provided data.

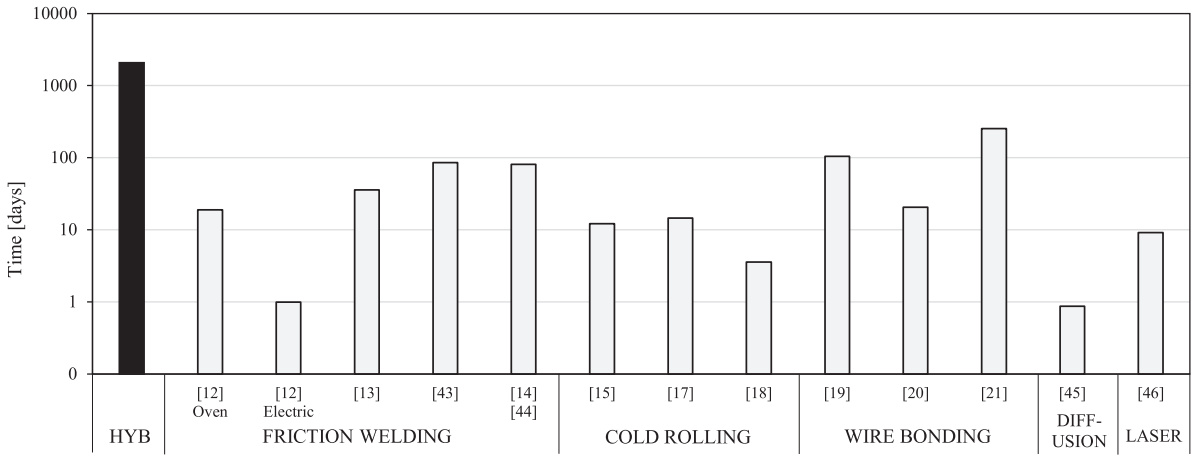

Fig. 15. Comparison of growth rates for different Al-Cu joining processes showing time taken for 2 μm of growth at 200 °C. Durations have been calculated based on reported activation energy and pre-exponential and compared to HYB results.

5.1. Future work

The negligible impact on electrical resistance and slow intermetallic growth are promising results of the potential functional performance. However, these initial results should be strengthened to fully characterise the functional performance of the HYB process for electrical conductors.

Assessment of structural integrity would be beneficial to confirm appropriate failure criteria. The electrical measurements in this study have shown that electrical resistance is not significantly impacted, even with an intermetallic thickness of 35 μm. However, the welds with a 35 μm thick IMP layer may have reduced structural integrity. Interestingly, despite the 2 μm criteria being widely cited, the criterion is mostly cited from two studies by Wallach & Davies [10] and Abbasi et al. [11]. The two studies are based on cold-rolled aluminum and copper and it would be useful to establish criteria specific for the butt welded HYB joints. Since fewer defects are suspected in the HYB weld it would be interesting to establish if this also improves the structural integrity. The structural characterisation should focus specifically on safety margin for electrical applications, such as bending and thermal fatigue. The characterisation should be performed versus intermetallic thickness to establish the design envelope for Al-Cu HYB welds.

In addition, continued testing of electrical resistance versus intermetallic thickness would be useful to establish the thickness at which electrical resistance is impacted. The maximum intermetallic thickness in this study was 35 μm and increasing to greater thickness may provide insight into the mechanisms causing electric resistance across weld interfaces. Moreover, additional artificial ageing should be conducted with electrical heating instead of using atmospheric heating from an oven. Braunovic & Alexandrov [12] and Solchenbach et al. [46] have shown that the diffusion rate is accelerated by electric current heating versus external heating. Therefore, establishing the diffusion rate from internal electric heating will be important for establishing the functional performance of the HYB process.

Declaration of competing interest

The authors declare that they have no known competing financial interests or personal relationships that could have appeared to influence the work reported in this paper.

References

[1] Gold R. Status report on electrification policy: where to next?. In: Current sustainable/renewable energy reports; 2021. p. 1–9.
[2] Zuo YY, Gong P, Ji SD, Li QH, Ma ZW, Lv Z. Ultrasound-assisted friction stir transient liquid phase spot welded dissimilar copper-aluminum joint. J Manuf Process 2021;62:58–66.
[3] Galvão I, Loureiro A, Rodrigues DM. Critical review on friction stir welding of aluminium to copper. Sci Technol Weld Join 2016;21(7):523–46.
[4] Messner F. Material substitution and path dependence: empirical evidence on the substitution of copper for aluminum. Ecol Econ 2002;42(1–2):259–71.
[5] Green HE. Aluminium in the electrical industry. Electron Power 1973;19(19): 473–5.
[6] Lee SS, Kim TH, Hu SJ, Cai WW, Abell JA. Joining technologies for automotive lithium-ion battery manufacturing: a review. In: International manufacturing science and engineering conference. Vol. 49460; 2010. p. 541–9.
[7] Slade PG. Electrical contacts: principles and applications. 2nd Edition. CRC press; 2017.
[8] Jackson RL. Electrical performance of aluminium/copper bolted joints. In: IEE proceedings C (generation, transmission and distribution). Vol. 129. IET; 1982. p. 177–84.
[9] Kah P, Vimalraj C, Martikainen J, Suoranta R. Factors influencing Al-cu weld properties by intermetallic compound formation. Int J Mech Mater Eng 2015;10 (1):1–13.
[10] Wallach ER, Davies GJ. Mechanical properties of aluminium-copper solid-phase welds. Metals Technol 1977;4(1):183–90.
[11] Abbasi M, Taheri AK, Salehi MT. Growth rate of intermetallic compounds in Al/Cu bimetal produced by cold roll welding process. J Alloys Compd 2001;319(1–2): 233–41.
[12] Braunovic M, Alexandrov N. Intermetallic compounds at aluminum-to-copper electrical interfaces: effect of temperature and electric current. IEEE Trans Compon Packag Manuf Technol Part A 1994;17(1):78–85.
[13] Lee W-B, Bang K-S, Jung S-B. Effects of intermetallic compound on the electrical and mechanical properties of friction welded Cu/Al bimetallic joints during annealing. J Alloys Compd 2005;390(1–2):212–9.
[14] P. Li L. Pan X. Hao S. Li H. Dong , Effect of post-weld heat treatment on inhomogeneity of aluminum/copper rotary friction welded joint, Mater Res Express 5 (9).
[15] Chen C-Y, Hwang W-S. Effect of annealing on the interfacial structure of aluminum-copper joints. Mater Trans 2007;48(7):1938–47. The Japan Institute of Metals.
[16] Hua F-A, Song H-W, Sun T, Li J-P. Inter-diffusion based analytical model for growth kinetics of IMC layers at roll bonded Cu/Al interface during annealing process. Met Mater Int 2020;26(3):333–45.
[17] Hilz E, Dudziak S, Schmid-Fetzer R. Formation and properties of intermetallic compounds in an Al-Cu roll-bonded connection. In: ICEC 2014; The 27th international conference on electrical contacts, VDE; 2014. p. 1–6.
[18] Li H, Yang Y, Liang X, Zhang W, Cao L, Wu C, Zeng Z, Wang L. Effect of annealing temperature and time on the microstructure, mechanical properties and conductivity of cold-rolled explosive Cu/Al composite sheets. Mater Res Express 2020;7(10).
[19] Kim H-J, Lee JY, Paik K-W, Koh K-W, Won J, Choe S, Lee J, Moon J-T, Park Y-J. Effects of Cu/Al intermetallic compound (IMC) on copper wire and aluminum pad bondability. IEEE Trans Compon Packag Technol 2003;26(2):367–74.
[20] Xu H, Liu C, Silberschmidt VV, Chen Z. Growth of intermetallic compounds in thermosonic copper wire bonding on aluminum metallization. J Electron Mater 2010;39(1):124–31.
[21] Liu C-P, Chang S-J, Liu Y-F, Chen W-S. Cu-Al interfacial formation and kinetic growth behavior during HTS reliability test. J Mater Process Technol 2019;267: 90–102.
[22] Grong Ø, Sandnes L, Berto F. A status report on the hybrid metal extrusion & bonding (HYB) process and its applications. Mater Des Process Commun 2019;1(2).

[23] Grong Ø, Sandnes L, Ferro P, Berto F. Chapter 9 - hybrid metal extrusion & bonding. In: Pereira MDB, da Silva FJG, editors. Handbook of welding: processes, control and simulation. Nova Science Publishers; 2021.
[24] Sandnes L. On the mechanical integrity of welded joints made by hybrid metal extrusion and bonding. Ph.D. thesis. Trondheim: Norwegian University of Science and Technology; 2021.
[25] Turgun H. Electron microscopy characterization of aluminium-copper-titanium-steel joint made using the hybrid metal extrusion & bonding method. NTNU; 2020. Master's thesis.
[26] Peña FDL, Prestat E, Fauske VT, Burdet P, Lähnemann J, Furnival T, Jokubauskas P, Nord M, Ostasevicius T, MacArthur KE, Johnstone DN, Sarahan M, Aarholt T, Taillon J, pquinn dls, Migunov V, Eljarrat A, Caron J, Poon T, Mazzucco S, Francis C, Martineau B, Somnath S, Slater T, Tappy N, Walls M, Cautaerts N, Winkler F, Actions user. DENSmerijn, hyperspy/hyperspy: release v1.6.5. URL, https://zenodo.org/record/5608741; Oct. 2021. https://doi.org/10.5281/zenodo.5608741.
[27] Zhang J, Wang B-H, Chen G-H, Wang R-M, Miao C-H, Zheng Z-X, Tang W-M. Formation and growth of Cu–Al IMCs and their effect on electrical property of electroplated Cu/Al laminar composites. Trans Nonferrous Metals Soc China 2016;26(12):3283–91.
[28] Ólafsson D, Vilaça P, Vesanko J. Multiphysical characterization of FSW of aluminum electrical busbars with copper ends. Weld World 2020;64(1):59–71.
[29] Wang X-G, DongYuan X, Li J-N, Li X-G. Influence of interfacial inter-metallic compounds on the electrical characterization of Cu/Al joints produced by flash welding and diffusion brazing. Mater Res 2020;23.
[30] Eslami N, Harms A, Henke B, Fricke A, Böhm S. Electrical and mechanical properties of friction stir welded Al-Cu butt joints. Weld World 2019;63(3):903–11.
[31] Savolainen K, Mononen J, Saukkonen T, Hänninen H. A preliminary study on friction stir welding of dissimilar metal joints of copper and aluminium. In: 6th international friction stir welding symposium; 2006. p. 10.
[32] Zhang H, Shi Y, Gu Y, Li C. Effect of different filler wires on mechanical property and conductivity of aluminum-copper joints. Materials 2020;13(16).
[33] Solchenbach T, Plapper P, Cai W. Electrical performance of laser braze-welded aluminum–copper interconnects. J Manuf Process 2014;16(2):183–9.
[34] Dimatteo V, Ascari A, Fortunato A. Continuous laser welding with spatial beam oscillation of dissimilar thin sheet materials (Al-Cu and Cu-Al): Process optimization and characterization. J Manuf Process 2019;44:158–65.
[35] Shaikh UF, Das A, Barai A, Masters I. Electro-thermo-mechanical behaviours of laser joints for electric vehicle battery interconnects. In: 2019 electric vehicles international conference (EV), IEEE; 2019. p. 1–6.
[36] Sharma N, Khan ZA, Siddiquee AN, Shihab SK, Wahid MA. Effect of process parameters on microstructure and electrical conductivity during FSW of Al-6101 and pure copper. Mater Res Express 2018;5(4).
[37] Berger HH. Contact resistance and contact resistivity. J Electrochem Soc 1972;119(4):507.
[38] Madhusudana CV. Thermal contact conductance. Mechanical Engineering Series. Cham: Springer International Publishing; 2014.
[39] Pfeifer S, Großmann S, Freudenberger R, Willing H, Kappl H. Characterization of intermetallic compounds in Al-Cu-Bimetallic interfaces. In: 2012 IEEE 58th Holm conference on electrical contacts (Holm), IEEE; 2012. p. 1–6.
[40] García-Navarro D, Ortiz-Cuellar JC, Galindo-Valdés JS, Gómez-Casas J, Muñiz-Valdez CR, Rodríguez-Rosales NA. Effects of the FSW parameters on microstructure and electrical properties in Al 6061-T6-Cu C11000 plate joints. Crystals 2021;11(1):21.
[41] Kidson GV. Some aspects of the growth of diffusion layers in binary systems. J Nucl Mater 1961;3(1):21–9.
[42] Gueydan A, Domengès B, Hug E. Study of the intermetallic growth in copper-clad aluminum wires after thermal aging. Intermetallics 2014;50:34–42.
[43] Xue P, Xiao BL, Ma ZY. Effect of interfacial microstructure evolution on mechanical properties and fracture behavior of friction stir-welded Al-Cu joints. Metall Mater Trans A 2015;46(7):3091–103.
[44] Pan L, Li P, Hao X, Zhou J, Dong H. Inhomogeneity of microstructure and mechanical properties in radial direction of aluminum/copper friction welded joints. J Mater Process Technol 2018;255:308–18.
[45] Guo Y, Liu G, Jin H, Shi Z, Qiao G. Intermetallic phase formation in diffusion-bonded Cu/Al laminates. J Mater Sci 2011;46(8):2467–73.
[46] Solchenbach T, Plapper P, Greger M, Biagi J-L, Bour J, Bomfim JAS. Thermal and electrical aging of laser braze-welded aluminum–copper interconnects. Transl Mater Res 2014;1(1).
[47] Wang X-G, Li X-G, Yan F-J, Wang C-G. Effect of heat treatment on the interfacial microstructure and properties of Cu-Al joints. Weld World 2017;61(1):187–96.
[48] Dalgaard E, Wanjara P, Trigo G, Jahazi M, Comeau G, Jonas JJ. Linear friction welding of Al–Cu part 2–interfacial characteristics. Can Metall Q 2011;50(4):360–70.
[49] Kemsies RH, Milkereit B, Kessler O, Fuhrmann T, Schlegel S, Plonus F, Miller-Jupp SP, Hirsch J. Effect of dispersoids on long-term stable electrical aluminium connections. In: Materials science forum. Vol. 877. Trans Tech Publ; 2017. p. 409–15.